

Showcasing research from Dr. Wojciech A. Sławiński and Prof. Krzysztof Wozniak laboratory, Faculty of Chemistry, University of Warsaw.

Charge density studies of single and transient (single to double) boron–oxygen bonds in $(\text{NH}_4)_2\text{B}_4\text{O}_5(\text{OH})_4 \cdot 2\text{H}_2\text{O}$

The investigated ion of $\text{H}_4\text{B}_4\text{O}_9^{2-}$ which makes up the $(\text{NH}_4)_2\text{B}_4\text{O}_5(\text{OH})_4 \cdot 2\text{H}_2\text{O}$ crystal structure consists of two types of boron atom. One of them, creates four regular single B–O bonds. The other one only three, but their character is transient, between single and double bond. Differences are clearly visible on the basis of experimental electron density distribution. Charge density and Laplacian at bond critical points show distinguishable values.

As featured in:



See Wojciech A. Sławiński *et al.*, *Dalton Trans.*, 2022, **51**, 14865.

Cite this: *Dalton Trans.*, 2022, **51**, 14865

Charge density studies of single and transient (single to double) boron–oxygen bonds in $(\text{NH}_4)_2\text{B}_4\text{O}_5(\text{OH})_4 \cdot 2\text{H}_2\text{O}^\dagger$

Roman Gajda,  Anna Piekara,  Daniel Tchoń,  Krzysztof Woźniak  and Wojciech A. Sławiński *

A $\text{H}_4\text{B}_4\text{O}_9^{2-}$ ion which makes up the $(\text{NH}_4)_2\text{B}_4\text{O}_5(\text{OH})_4 \cdot 2\text{H}_2\text{O}$ crystal structure has two types of boron–oxygen bonds, *i.e.* single B–O bonds and an intermediate between single and double B \equiv O bonds. Differences between these two bond types are visible not only because they differ by their lengths but also a topology of electron density distribution differs. This also gives a hint as to how to distinguish between these two bond types. Experimental results based on multipole model refinement gave excellent agreement with theoretical calculations and literature data. Calculations at bond critical points for B–O and B \equiv O (electron density, the Laplacian of electron density and the localized-orbital locator function) suggest us how boron–oxygen bonds should be categorised with respect to compounds previously reported in the literature. Additionally, a novel synthesis method for the investigated compound has been developed, which involves crystallization from an aqueous solution of BH_3NH_3 dissolved in a mixture of tetrahydrofuran and water.

Received 27th July 2022,
Accepted 6th September 2022

DOI: 10.1039/d2dt02442j

rsc.li/dalton

Introduction

Issues in boron chemistry are still less well-addressed than those of the chemistry of carbon. One of such issues involves bonds between boron and oxygen. It is already known that in addition to single, double and triple B–O bonds, there also exists a type of boron intermediate between a single and double bond¹ called here a transient single to double bond. To analyze this phenomenon topologically, DFT calculations were performed and electron localisation functions (ELF) were measured in a wide set of relatively simple molecules containing boron.^{2–4} These theoretically optimized structures were also characterized by their properties at the bond critical points (BCPs).

In this paper, along with examining the $\text{H}_4\text{B}_4\text{O}_9^{2-}$ ion, we will look deeper into the phenomena of B–O and B \equiv O bonds. The results presented here originate from high-resolution, single crystal X-ray diffraction experiments. Collection of high quality data allowed us to obtain experimental charge density

distributions. Multipole model refinement according to the Hansen–Coppens theory was adopted. Experimental data were analyzed and compared with theoretical DFT based calculations.

Results and discussion

Synthesis

Ammonia borane BH_3NH_3 (borane-ammonia complex; CAS number 13774-81-7; 97% from Sigma-Aldrich) was dissolved in a mixture of water and tetrahydrofuran (THF) (tetrahydrofuran CZDA, ACS; CAS number 109-99-9; 99.8% from POCH) according to:⁵



THF was chosen for the high solubility of ammonia borane in it and its volatility.⁶ The mixture was sealed and allowed to stand at room temperature for 7 days. After this time, crystals of $(\text{NH}_4)_2\text{B}_4\text{O}_5(\text{OH})_4 \cdot 2\text{H}_2\text{O}$ began to form at the bottom of the vessel.

Experimental

X-ray measurements were conducted at 90 K on an in-house SuperNova diffractometer (molybdenum X-ray source) equipped with a new direct photon counting device (HyPix 6000HE HPC). The images were processed with CrysAlis.⁷ The

Faculty of Chemistry, University of Warsaw, Pasteura 1, 02-093 Warsaw, Poland.

E-mail: wslawinski@chem.uw.edu.pl

[†] Electronic supplementary information (ESI) available: Normal distribution of residual electron density plots, structure factors as a function of $\sin \theta/\lambda$ and fractal plots for residual density for both experimental and theoretical data. Finally, a normal probability plot is presented for experimental data. CCDC 2181471 and 2181472. For ESI and crystallographic data in CIF or other electronic format see DOI: <https://doi.org/10.1039/d2dt02442j>



structures were solved and refined with ShelXS⁸ and ShelXL⁹ within the Olex2 suite.¹⁰ Details of the X-ray experiment are presented in Table 1. Atomic positions obtained from a spherical model (Independent Atom Model – IAM) are shown in Table 2. These spherical model (Independent Atom Model – IAM) served as the starting point for the refinement of the Hansen–Coppens multipole model of electron density.^{11,12} In the multipole model the total atomic electron density in the crystal is treated as a sum of atomic contributions centered at the atomic positions. Each of the atomic contributions consists of the following three components:

$$\rho(r) = \rho_c(r) + P_{\text{val}}\kappa^3\rho_v(\kappa r) + \sum_{m=0}^l \kappa^3 R_l(\kappa' r) \sum_{m=0}^l P_{lm\pm} d_{lm\pm}(\theta, \varphi)$$

In this equation, $\rho_c(r)$ and $\rho_v(r)$ are spherical core and valence densities. The third term contains the sum of the

angular functions $d_{lm\pm}(\theta, \varphi)$ to take into account the aspherical deformations. The angular functions $d_{lm\pm}(\theta, \varphi)$ are real spherical harmonic functions. The coefficients P_{val} and $P_{lm\pm}$ are multipole populations for the valence and deformation density multipoles. κ and κ' are scaling parameters which describe whether valence and deformation densities are expanding or contracting. In the Hansen–Coppens formalism, P_{val} , $P_{lm\pm}$, κ and κ' are refineable parameters together with the atomic coordinates and thermal displacement coefficients. The XD2016 program package was used to conduct multipole model refinement.¹³ For both experimental and theoretical data the same approach has been applied. Multipoles of non-hydrogen atoms were refined up to hexadecapoles, whereas hydrogen atoms were refined up to dipoles only. Because all atoms are placed at general positions, no special positions are involved and no constraints for any multipoles were used. Parameters κ were refined for all types of atoms and κ' was set to 1. The length of the O–H bonds was constrained as 0.96 Å. The anisotropic thermal parameters of hydrogen atoms were calculated using so called SHADE3 (Simple Hydrogen Anisotropic Displacement Estimator).¹⁴

Calculations

Experimental X-ray measurements were conducted at a low temperature (90 K) accompanied by theoretical calculations.

Table 1 (NH₄)₂B₄O₅(OH)₄·2H₂O crystal structure and single crystal X-ray diffraction experimental details

Spherical refinement	
Crystal system, space group	Monoclinic, <i>P</i> 2 ₁
<i>a</i> , <i>b</i> , <i>c</i> (Å)	7.16499(7), 10.59066(11), 7.24742(6)
β (°)	98.6290(9)
<i>V</i> (Å ³)	543.72(1)
<i>Z</i>	2
<i>F</i> (000)	276.244
<i>D_x</i> (Mg m ⁻³)	1.609
Radiation type	MoK α
No. of reflections for cell measurement	51 795
θ range (°) for cell measurement	3.5–65.9
μ (mm ⁻¹)	0.16
Data collection	
Diffraction	SuperNova, Dual, HyPix 6000HE
Scan method	HPC
Absorption correction	ω scans
<i>T</i> _{min} , <i>T</i> _{max}	0.738, 1.000
Measur., independ., observ. [<i>I</i> ≥ 2 σ (<i>I</i>)] refl.	94 540, 17 621, 15 709
<i>R</i> _{int}	0.056
θ values (°)	$\theta_{\text{max}} = 62.7$, $\theta_{\text{min}} = 3.4$
($\sin \theta/\lambda$) _{max} (Å ⁻¹)	1.250
Range of <i>h</i> , <i>k</i> , <i>l</i>	<i>h</i> = −17→17, <i>k</i> = −26→26, <i>l</i> = −18→18
Refinement on	<i>F</i> ²
<i>R</i> [<i>F</i> ² > 2 σ (<i>F</i> ²)], <i>wR</i> (<i>F</i> ²), <i>S</i>	0.045, 0.114, 1.08
No. of reflections	17 621
No. of parameters	218
No. of restraints	10
Absolute structure	Hooft <i>et al.</i> ³⁵
Absolute structure parameter	−0.03 (14)

Multipole refinement	
Refinement on, parameters, reflections	<i>F</i> , 460, 13 460
<i>R</i> [<i>F</i> ² > 2 σ (<i>F</i> ²)], <i>R</i> (all)	0.039, 0.038
<i>wR</i> [<i>F</i> ² > 2 σ (<i>F</i> ²)], <i>S</i>	0.071, 1.156
Weighting scheme	$w = 1/[\sigma^2(F_o^2)]$
(Δ/σ) _{max}	0.015
$\Delta>_{\text{max}}$, $\Delta>_{\text{min}}$ (e Å ⁻³)	0.571, −0.308

Table 2 Atomic positions for the (NH₄)₂B₄O₅(OH)₄·2H₂O crystal structure (after independent atom model refinement)

Atom	Fract <i>x</i>	Fract <i>y</i>	Fract <i>z</i>
O(1)	0.06319(6)	0.44385(4)	0.68750(7)
O(2)	0.24306(6)	0.29958(5)	0.53000(7)
O(3)	0.31420(7)	0.44619(4)	0.95184(6)
O(4)	0.49498(7)	0.30342(5)	0.79399(6)
O(5)	0.37996(6)	0.49770(4)	0.64351(5)
O(6)	0.19981(7)	0.63914(4)	0.81436(6)
O(7)	0.56577(7)	0.35028(6)	0.49451(6)
O(8)	0.9144(7)	0.27897(5)	0.49693(7)
O(9)	0.49778(7)	0.29138(5)	0.12259(6)
O(10)	0.06317(19)	0.87621(9)	0.94202(19)
O(11)	0.14951(11)	0.11372(8)	0.85189(11)
B(1)	0.24174(8)	0.50941(5)	0.77181(8)
B(2)	0.42137(8)	0.36466(6)	0.61207(8)
B(3)	0.07436(8)	0.34303(6)	0.57214(8)
B(4)	0.43707(9)	0.34731(6)	0.95314(8)
N(1)	0.25347(7)	0.10041(5)	0.27331(8)
N(2)	0.27296(9)	0.59516(5)	0.12259(7)
H(1A)	0.160(4)	0.043(3)	0.297(4)
H(1B)	0.215(3)	0.124(2)	0.155(3)
H(1C)	0.255(5)	0.163(3)	0.345(5)
H(1D)	0.375(4)	0.062(3)	0.295(4)
H(2A)	0.296(3)	0.537(3)	0.188(3)
H(2B)	0.337(5)	0.650(3)	0.254(5)
H(2C)	0.157(4)	0.611(3)	0.252(4)
H(2D)	0.311(5)	0.573(3)	0.376(3)
H(6)	0.151(4)	0.684(3)	0.710(3)
H(7)	0.511(2)	0.3516(16)	0.4376(19)
H(8)	0.818(3)	0.304(3)	0.524(4)
H(9)	0.570(8)	0.221(4)	0.113(9)
H(10A)	0.086(3)	0.7876(19)	0.936(3)
H(10B)	0.107(7)	0.923(5)	0.848(5)
H(11A)	0.159(2)	0.0330(13)	0.848(2)
H(11B)	0.094(6)	0.173(4)	0.950(5)



These calculations had two goals. One was to obtain the topology of the electron density distribution in the investigated molecule only on the basis of density-functional theory (DFT). The other was to produce a list of theoretical structure factors, which could be used for multipole model refinement. Both approaches worked as a good benchmark for the multipole model refined with pure experimental data collected on an in-house diffractometer. For these DFT calculations we used the CRYSTAL17 program^{15,16} which is devoted to periodic system calculations and allows charge density topological analysis. We also used the B3LYP^{17,18} exchange–correlation functional corrected for dispersion by Grimme's D3¹⁹ correction in conjunction with the pob-TZVP-rev2 basis sets.²⁰ Calculations in CRYSTAL17 were conducted according to the following assumptions: (1) calculations will mimic experiments as much as possible so that unit cell parameters were fixed and equal to the corresponding experimental results obtained by X-ray measurement; (2) solvent molecules/ions (H_2O and NH_4^+) were treated as rigid groups. Theoretical dynamic structure factors were calculated with CRYSTAL17²¹ and later used to refine a multipolar model of the electron density using the XD2016 package.¹³ Structure factors obtained this way were refined with the multipole model. Additionally, also in this case the topological analysis of the theoretical charge density distributions was performed with TOPOND14^{22,23} as implemented in the CRYSTAL17 program package. As a result, theoretical calculations gave us two types of output. First, on the basis of constrained calculations (unit cell parameters were the same as those obtained from the experiment), sets of dynamic structure factors suitable for multipolar model refinement were produced. Second, charge density topological analysis was performed on the basis of fully theoretical input data (TOPOND14).

Results

The unit cell of $(\text{NH}_4)_2\text{B}_4\text{O}_5(\text{OH})_4 \cdot 2\text{H}_2\text{O}$ (see Fig. 1) consists of two ions of $\text{H}_4\text{B}_4\text{O}_9^{2-}$ and eight solvent molecules/ions: four H_2O and four NH_4^+ , half of which is in the asymmetric unit (see Fig. 2). As we see from Fig. 1, $\text{H}_4\text{B}_4\text{O}_9^{2-}$ ions are arranged into ribbon-like type layers. The space between such layers is filled in with solvent molecules, water and NH_4^+ cations and the whole structure is stabilised by $\text{O}-\text{H}\cdots\text{O}$ and $\text{N}-\text{H}\cdots\text{O}$ hydrogen bonds (see Table 3). Each $\text{H}_4\text{B}_4\text{O}_9^{2-}$ anion is connected *via* $\text{O}-\text{H}\cdots\text{O}$ and $\text{O}\cdots\text{H}-\text{O}$ contacts with eight neighbouring $\text{H}_4\text{B}_4\text{O}_9^{2-}$ ions (Fig. 1, right panel), which creates the main scaffolding. Additional $\text{N}-\text{H}\cdots\text{O}$ and $\text{O}-\text{H}\cdots\text{O}$ inter-

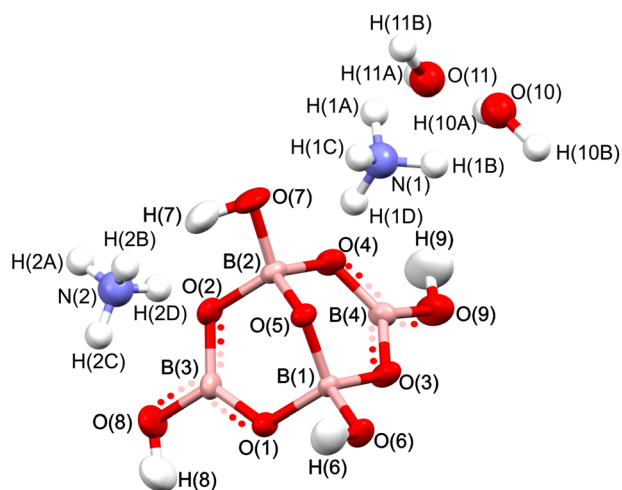


Fig. 2 $\text{H}_4\text{B}_4\text{O}_9^{2-}$ ion. Single B–O and transient B...O bonds are depicted by solid and dotted bond types, respectively.

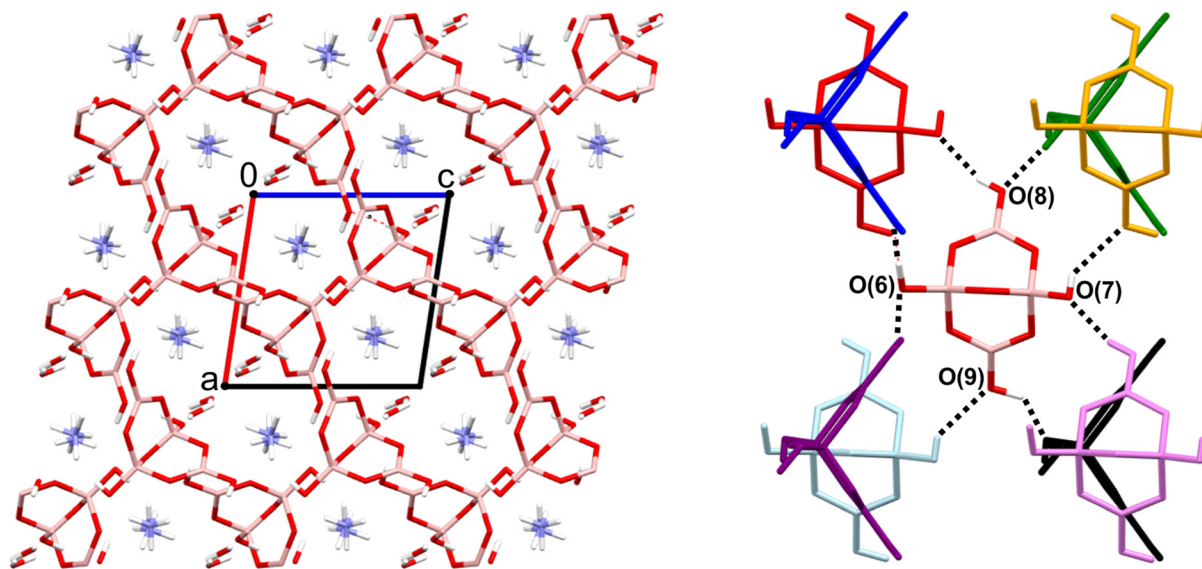


Fig. 1 Molecular arrangement in $(\text{NH}_4)_2\text{B}_4\text{O}_5(\text{OH})_4 \cdot 2\text{H}_2\text{O}$ – view along the b axis (left panel). Selected intermolecular hydrogen bonds, view along the $[111]$ direction (right panel). Symmetry codes: yellow: $x, y, z - 1$; green: $-x, y - 1/2, 1 - z$; navy blue: $-x, y + 1/2, 1 - z$; red: $x - 1, y, z$; black: $1 - x, y - 1/2, 2 - z$; violet: $x + 1, y, z$; light blue: $x, y, z + 1$; magenta: $1 - x, y + 1/2, 2 - z$ respectively.



Table 3 Geometry (distances and angles) of hydrogen bonds present in the $(\text{NH}_4)_2\text{B}_4\text{O}_5(\text{OH})_4 \cdot 2\text{H}_2\text{O}$ crystal structure (after independent atom model refinement)

Donor contact D–H	$d(\text{D–H})$ [Å]	$d(\text{H}\cdots\text{A})$ [Å]	<DHA angle [°]	$d(\text{D}\cdots\text{A})$ [Å]	Acceptor A	Symmetry code
O(6)–H(6)	0.920	1.805	172.85	2.720	O(8)	$-x, y + 1/2, -z + 1$
O(7)–H(7)	0.523	2.358	132.36	2.738	O(9)	$x, y, z - 1$
O(8)–H(8)	0.790	1.854	158.97	2.607	O(7)	$x - 1, y, z$
O(9)–H(9)	0.912	1.871	147.31	2.684	O(6)	$-x + 1, y - 1/2, -z + 1$
N(1)–H(1A)	0.939	1.930	169.66	2.858	O(1)	$-x, y - 1/2, -z + 1$
N(1)–H(1B)	0.896	2.178	160.27	3.036	O(11)	$x, y, z - 1$
N(1)–H(1C)	0.843	1.981	173.95	2.821	O(2)	
N(1)–H(1D)	0.948	1.878	174.90	2.823	O(5)	$-x + 1, y - 1/2, -z + 1$
N(2)–H(2A)	0.882	1.984	162.39	2.837	O(3)	
N(2)–H(2B)	0.757	2.083	177.49	2.839	O(4)	$-x + 1, y + 1/2, -z + 2$
N(2)–H(2C)	0.837	2.213	164.90	3.028	O(11)	$-x, y + 1/2, -z + 2$
N(2)–H(2D)	0.822	2.084	172.45	2.900	O(5)	$x, y, z + 1$
O(10)–H(10A)	0.955	2.033	149.63	2.897	O(6)	
O(10)–H(10B)	0.937	2.039	125.52	2.694	O(11)	$x, y + 1, z$
O(11)–H(11A)	0.858	1.958	143.08	2.694	O(10)	$x, y - 1, z$
O(11)–H(11B)	1.066	2.606	155.03	3.601	O(10)	$-x, y - 1/2, -z + 2$

actions connect it with solvent molecules. The position and orientation of solvent molecules experience some level of disorder, but its arrangement is out of the scope of our investigations. Our main focus in this paper is to describe the nature of boron/oxygen interactions and the bonds formed.

Boron/oxygen interactions were investigated to some extent by Straub (1995).¹ On the basis of bond lengths we can distinguish single B–O, double B=O, triple B≡O and transient B \cdots O bonds. The length of a single B–O bond is reported to be *ca.* 1.470 Å, whereas the length of transient bonds B \cdots O should vary between 1.360 Å and 1.386 Å. In the case of the $\text{H}_4\text{B}_4\text{O}_9^{2-}$ ion, there are fourteen boron–oxygen bonds. Their lengths are presented in Table 4. It can be clearly observed that there are two different groups of bonds. Atoms B(1) and B(2) create a B–O bond, whereas B(3) and B(4) form a B \cdots O bond. In Fig. 2, localisation of these bonds in the $\text{H}_4\text{B}_4\text{O}_9^{2-}$ ion is depicted by solid and dotted bonds, respectively.

The differences between B–O and B \cdots O should also be observable when we take into consideration properties such as electron density and the Laplacian of electron density at bond critical points (BCPs). Issues of BCPs are well defined by the quantum theory of atoms in molecules (QTAIM).^{24,25}

There is very little known about the distribution of charge density in B–O and B \cdots O bonds. The most recent paper by

Michalski *et al.* presents topological parameters for the B–O bonds obtained on the basis of DFT calculations in Gaussian.³ In the molecule investigated in that paper (ABEMID trimethylammonio-dicyano(methylmercapto)borate), properties at the bond critical points corresponding to B–O bonds have values as follows: electron density $\rho_{(3,-1)}(r) = 1.236$ ($\text{e} \text{ \AA}^{-3}$) and Laplacian $\nabla^2\rho_{(3,-1)}(r) = 16.519$ ($\text{e} \text{ \AA}^{-5}$). A positive value of the Laplacian in conjunction with a relatively large value of $\rho_{(3,-1)}(r)$ suggest that the bond has dative character. The same paper also investigated 27 molecules with a B–S bond which has been selected from the CSD database and the calculations were performed for their derivatives whereas the S atom has been replaced by an O atom. In that set of molecules the average values of properties at bond critical points were as follows: $\rho_{(3,-1)}(r)$ varied between 0.896 and 1.383 ($\text{e} \text{ \AA}^{-3}$) and the Laplacian $\nabla^2\rho_{(3,-1)}(r)$ varied between 12.417 and 22.406 ($\text{e} \text{ \AA}^{-5}$). It must be emphasised that these results are only based on DFT calculations, whereas the results presented in our paper have their origins in experimental data.

In Table 5 we compare values of electron density and the Laplacian obtained for B–O and B \cdots O bonds which exist in the $\text{H}_4\text{B}_4\text{O}_9^{2-}$ ion. The results from multipole model refinement based on experimental data (XD exp. data) are compared with the multipole model refinement based on theoretical dynamic structure factors (XD theor. data) and with the topology of electron density obtained directly from DFT calculations in CRYSTAL17 (Topond14). As we see from Table 5, just by comparing the values of $\rho_{(3,-1)}(r)$ and $\nabla^2\rho_{(3,-1)}(r)$ we can clearly distinguish whether a particular boron oxygen interaction is a B–O or B \cdots O bond. For B–O, the electron density (XD theor. data) at BCPs is lower and varied from 0.97 to 1.08 $\text{e} \text{ \AA}^{-3}$ (with an average of 1.04 $\text{e} \text{ \AA}^{-3}$), whereas for B \cdots O it varied from 1.30 to 1.46 $\text{e} \text{ \AA}^{-3}$ (with the average of 1.40 $\text{e} \text{ \AA}^{-3}$). As a consequence, the second derivative of electron density – Laplacian – showed significant differences. Generally speaking, the Laplacian for B–O was lower than 10 ($\text{e} \text{ \AA}^{-5}$), whereas for B \cdots O it was higher than 10 ($\text{e} \text{ \AA}^{-5}$). The results of $\rho_{(3,-1)}(r)$ and $\nabla^2\rho_{(3,-1)}(r)$ obtained

Table 4 B–O bond lengths in the $\text{H}_4\text{B}_4\text{O}_9^{2-}$ ion

Bond	Length [Å]	Bond	Length [Å]
B(1)–O(1)	1.5025(7)	B(3)–O(1)	1.3659(7)
B(1)–O(3)	1.4889(7)	B(3)–O(2)	1.3700(7)
B(1)–O(5)	1.4619(7)	B(3)–O(8)	1.3724(7)
B(1)–O(6)	1.4494(7)	B(4)–O(3)	1.3673(7)
B(2)–O(2)	1.4944(8)	B(4)–O(4)	1.3647(7)
B(2)–O(4)	1.4928(7)	B(4)–O(9)	1.3740(7)
B(2)–O(5)	1.4647(8)		
B(2)–O(7)	1.4436(7)		



Table 5 Values of properties at (3,−1) BCPs

B–O	Topond14		XD exp. data		XD theor. data	
	$\rho_{(3,-1)}(r)$ [$e \text{ \AA}^{-3}$]	$\nabla^2\rho_{(3,-1)}(r)$ [$e \text{ \AA}^{-5}$]	$\rho_{(3,-1)}(r)$ [$e \text{ \AA}^{-3}$]	$\nabla^2\rho_{(3,-1)}(r)$ [$e \text{ \AA}^{-5}$]	$\rho_{(3,-1)}(r)$ [$e \text{ \AA}^{-3}$]	$\nabla^2\rho_{(3,-1)}(r)$ [$e \text{ \AA}^{-5}$]
B(1)–O(1)	1.026	8.435	1.21(5)	−1.7(2)	0.97(1)	9.37(5)
B(1)–O(3)	1.073	9.326	1.24(5)	−0.6(2)	1.04(1)	8.32(5)
B(1)–O(5)	1.127	8.868	1.24(5)	0.8(2)	1.08(1)	8.18(4)
B(1)–O(6)	1.080	9.326	1.25(5)	2.0(2)	1.01(1)	11.56(5)
B(2)–O(2)	1.019	8.314	1.08(5)	2.6(2)	1.05(1)	4.43(5)
B(2)–O(4)	1.019	8.266	1.02(5)	9.2(2)	1.00(1)	8.23(5)
B(2)–O(5)	1.120	8.796	1.14(5)	7.0(2)	1.10(1)	5.56(5)
B(2)–O(7)	1.134	10.218	1.53(5)	−9.8(2)	1.05(1)	12.67(5)
Average	1.075	8.939	1.21(2)	1.19(1)	1.04(1)	8.54(2)
B\cdotsO						
B(3)–O(1)	1.437	17.761	1.46(5)	12.5(3)	1.40(1)	18.56(6)
B(3)–O(2)	1.410	16.773	1.35(5)	20.9(3)	1.39(1)	12.84(6)
B(3)–O(8)	1.323	15.809	1.70(5)	−2.4(3)	1.30(1)	10.53(6)
B(4)–O(3)	1.431	17.472	1.44(5)	14.8(3)	1.46(1)	11.72(6)
B(4)–O(4)	1.417	17.158	1.57(5)	6.8(3)	1.44(1)	12.49(6)
B(4)–O(9)	1.336	15.881	1.35(5)	9.1(3)	1.38(1)	10.17(6)
Average	1.392	16.809	1.48(2)	10.28(1)	1.40(1)	12.72(2)

on the basis of the theoretical dynamic structure factors were in good agreement with those obtained directly from DFT calculations. However, taking the multipole refinement of experimental data into consideration we see that although the values of $\rho_{(3,-1)}(r)$ still correspond very well to the experimental data, the Laplacian was a little bit biased. The results presented in this paper do not contradict recent theoretical calculations but rather are complementary. It must be underlined that the origin of all the datasets investigated in this study was a single crystal X-ray diffraction measurement. Calculations of multipole model refinement in XD take into account the whole crystal structure, including the surrounding solvent molecules. Also Crystal17, which is a source of dynamic theoretical structure factors and a starting point for further Topond14 calculations is devoted to periodic system calculations. That is why it is obvious that some differences with the literature data obtained from the DFT calculations of the gas phase molecule must appear. However, we believe that the results presented in this paper (based on diffraction experiments), in particular values of $\rho_{(3,-1)}(r)$ and $\nabla^2\rho_{(3,-1)}(r)$, will work much better to classify some future structures containing boron/oxygen interactions. It will enable the assignment of B–O or B \cdots O bond type.

In the literature, charge density has already been described in the case of several structures containing boron.^{26–29} Although some of them include B–O, those manuscripts were not directly focused on the bond charge and types. However, information about the properties at BCPs of such bonds (see Table 6) is presented in some of them. For example, Durka *et al.*²⁶ compared the experimental and theoretical data for two boron–oxygen bonds. On the basis of what we have already observed the comparison of those data with our findings appears interesting. Experimental values (bond length, density, and Laplacian) suggest that both of them are just single B–O bonds. Whereas on the basis of the theoretical values of bond length and Laplacian we would rather categorise them as B \cdots O bond type. Anyway, experimental and theoretical results seem to be inconsistent in this case. In the second example, the paper written by Jarzemska *et al.*,²⁷ there are four boron–oxygen bonds. Two of the bond lengths were longer than 1.46 Å, with the value of charge density being *ca.* 1 $e \text{ \AA}^{-3}$ and its Laplacian being $<10 e \text{ \AA}^{-5}$. It is clear that these bonds should be considered as a single B–O bond. On the other hand, the two other bonds are significantly shorter ($d < 1.4 \text{ \AA}$) and the Laplacian is $>10 e \text{ \AA}^{-5}$ and the density varied between 1.3 and 1.4 $e \text{ \AA}^{-3}$. These bonds should be categorised as B \cdots O.

Table 6 Parameters of properties at (3,−1) BCPs taken from the literature^{26,27}

Bond	Experimental			Theoretical		
	length [\AA]	$\rho_{(3,-1)}(r)$ [$e \text{ \AA}^{-3}$]	$\nabla^2\rho_{(3,-1)}(r)$ [$e \text{ \AA}^{-5}$]	length [\AA]	$\rho_{(3,-1)}(r)$ [$e \text{ \AA}^{-3}$]	$\nabla^2\rho_{(3,-1)}(r)$ [$e \text{ \AA}^{-5}$]
1 B–O ²⁶	1.4544(3)	1.21(2)	5.7(1)	1.376	1.29	25.79
2 B–O ²⁶	1.4428(3)	1.26(2)	6.6(1)	1.375	1.30	25.93
3 B–O ²⁷	1.4985(3)	1.1	6.9			
4 B–O ²⁷	1.4678(4)	1.1	9.6			
5 B–O ²⁷	1.3892(4)	1.3	13.4			
6 B–O ²⁷	1.3509(4)	1.4	18.9			



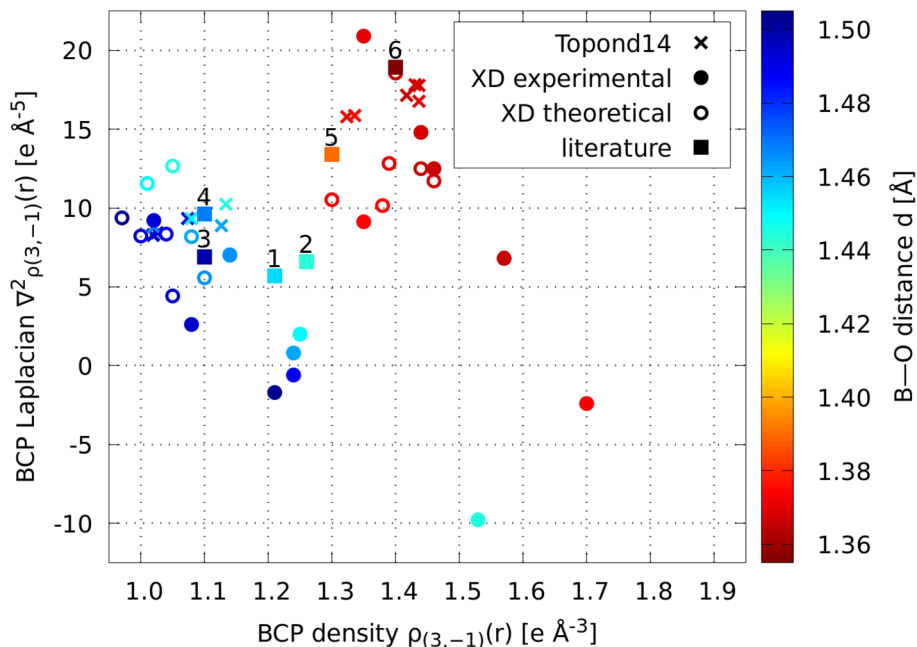


Fig. 3 Comparison of the electron density and its Laplacian at bond critical points corresponding to B–O (bluish region) and B≡O (reddish area) bond types. Colorful scale corresponds to the length of the boron–oxygen bond. Numbers 1–6 correspond to the literature data from Table 6.

Fig. 3 presents the comparison of properties at BCPs such as the electron density and its Laplacian obtained from both experimental and theoretical data. Selected literature data (corresponding to Table 6) are also included. As we see it is easily possible to distinguish zones which correspond to particular types of bonds, B–O (bluish region) and B≡O (reddish area) respectively. As was already mentioned above, in the case of B–O bonds values of charge densities vary between 1.0 and 1.3 e Å⁻³, whereas for B≡O, the charge density is more likely between 1.3 and 1.5 e Å⁻³. Laplacian, except for some outliers, have positive values. For B–O bonds, the values of Laplacian are mostly between 5 and 10 e Å⁻⁵ and between 10 and 20 for B≡O bonds.

Fig. 4 presents the topology of the electron density distribution in the vicinity of the B(3) atom. The hydrogen atom H(8) is off plane. All three B≡O bonds: B(3)–O(1), B(3)–O(2) and B(3)–O(8) lay in the plane of the figure. Pictures compare the results obtained on the basis of multipole model refinement (XD2016) conducted on the basis of experimental (X-ray measurement) and theoretical (CRYSTAL17) data. In the first row of Fig. 4 gradient lines of the electron density are presented. Blue circles represent bond critical points whereas green circles show ring critical points. According to the atoms in molecules theory,²⁴ each atom is considered with its atomic basin. It is simply a space where the paths of the gradient vectors of the electron density terminate in a given nucleus. The shape of a particular basin is defined by its neighboring atoms and is open at the exterior of the molecule. The gradient paths do not cross the boundaries of the basins. The atom zones are closed by a zero-flux surface surrounding each atom in the molecule. Partition of molecules into such zones is pre-

sented in the first row of Fig. 4. Contour values for the residual density and deformation density are 0.05 e Å⁻³. For the Laplacian maps, particular contours are ±2, 4, 8, 20, 40, 80, 200, 400 and 1000 e Å⁻⁵. Blue contours denote positive values and red contours correspond to negative values. On deformation density maps, solid blue lines show electron concentration, whereas dotted red lines denote the depletion of electrons. One can easily find a positive value of Laplacian in the middle of the trace of each B≡O bond. On the map of the deformation density the free electron pairs of O(1), O(2) and O(8) are visible.

It is worthy underlining that in the case of theoretical data the residual density map is almost absolutely flat, whereas in the case of experimental data the situation is different. The charts presented in the ESI† show that in both cases, experimental and theoretical, the residual electron density has a normal distribution (see Fig. 1 in the ESI†). However, even if it is randomly spread across the map, it can still affect the contours, especially if it is relatively high as in the experimental data case. Charts of the fractal distribution of the residual electron density presented in the ESI (Fig. 3†) show that peaks and holes on the residual density maps are equal or less than 0.2 e Å⁻³, whereas in the case of experimental data they vary between 0.3 and -0.6 e Å⁻³. Maps obtained on the basis of theoretical calculations show us what we would obtain if the experimental data were measured without any errors.

The topology presented in Fig. 5 looks similar. Four B–O type bonds, lying in a plane, are presented: B(1)–O(6), B(1)–O(5), B(2)–O(7) and B(2)–O(5). Laplacian maxima are visible at *ca.* the mid-points of bond paths. The deformation density maps also show the electron which belongs to the free electron pairs of oxygen atoms.



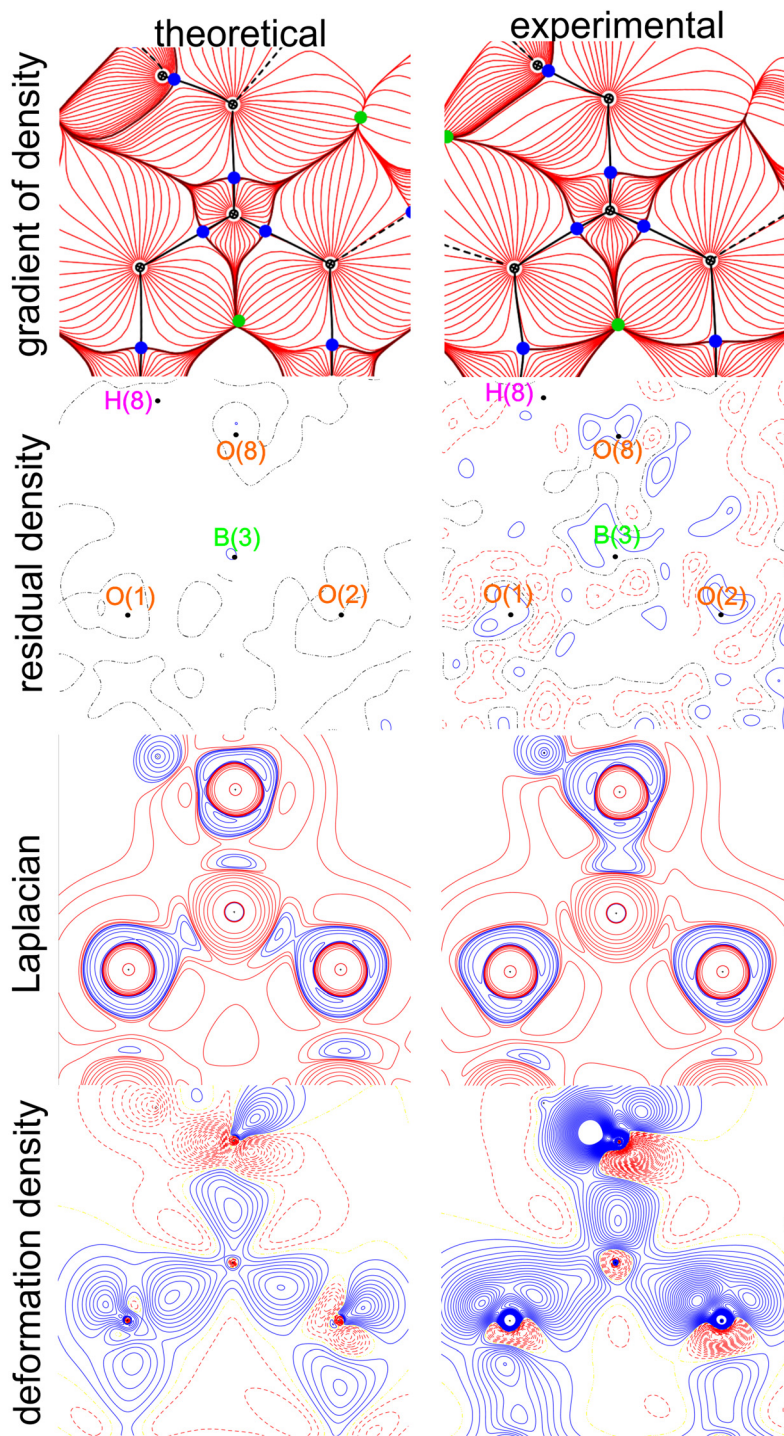


Fig. 4 Comparison of the results obtained on the basis of multipole model refinement (XD2016) conducted on the basis of experimental (X-ray measurement) and theoretical (CRYSTAL17) data: gradient of density, residual density, Laplacian and deformation density calculated on a plane defined by oxygen atoms around the central boron atom in the $\text{H}_4\text{B}_4\text{O}_9^{2-}$ ion. $\text{B}=\text{O}$ type bonds are depicted. On the top panels, blue and green circles represent bond critical points and ring critical points, respectively.

For the $\text{H}_4\text{B}_4\text{O}_9^{2-}$ ion, B–O type bonds are formed by boron atoms B(1) and B(2). As shown in Fig. 2, each of these boron atoms formed four such bonds (tetragonal arrangement). B(3) and B(4) atoms create $\text{B}=\text{O}$ type bonds and each of them formed three such bonds (flat arrangement). It is expected

that the boron atoms within the tetragonal arrangement would have different atomic charges than boron atoms connected to three oxygen atoms. Indeed, as we see from Table 7, the net atomic charges of integrated atomic basins corresponding to B(1) and B(2) were equal to +1.96 and +2.13 e, respectively. In



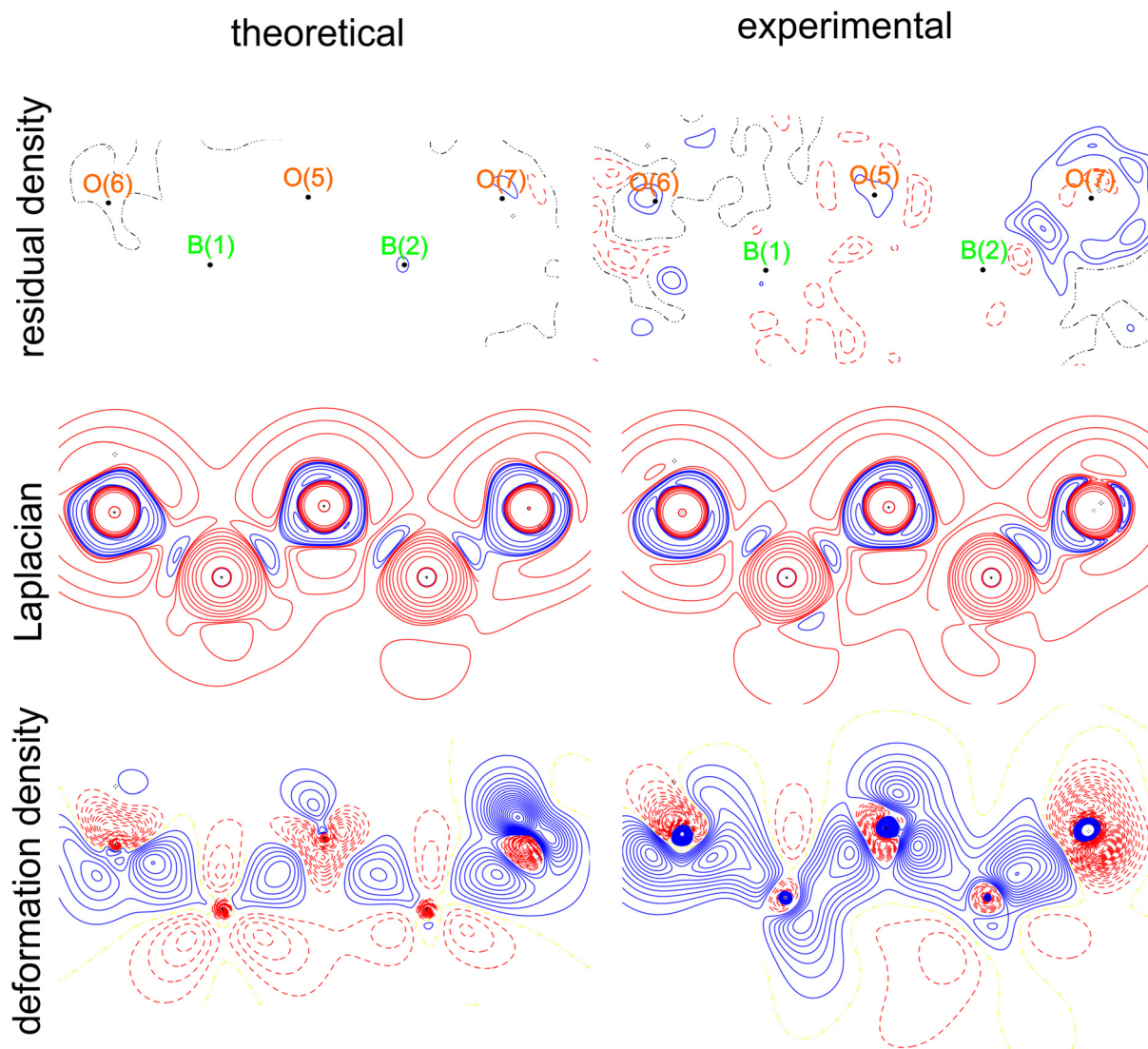


Fig. 5 Comparison of the results obtained on the basis of multipole model refinement (XD2016) conducted on the basis of experimental (X-ray measurement) and theoretical (CRYSTAL17) data: residual density, Laplacian and deformation density calculated on a plane defined by B(1), B(2) and O(7) atoms in the $\text{H}_4\text{B}_4\text{O}_9^{2-}$ ion.

Table 7 Charges of integrated atomic basins for boron and oxygen atoms in the $\text{H}_4\text{B}_4\text{O}_9^{2-}$ ion

Atom	Charge [e]	Atom	Charge [e]
B(1)	1.96	O(6)	-1.35
B(2)	2.13	O(7)	-1.4
B(3)	2.27	O(8)	-1.5
B(4)	2.21	O(9)	-1.65
O(1)	-2.00		
O(2)	-1.75		
O(3)	-1.86		
O(4)	-1.61		
O(5)	-1.60		

the case of B(3) and B(4), the net charges of atomic basins were slightly but noticeably higher and vary between +2.21 and +2.27 e. Boron atoms surrounded by four oxygen atoms

(forming B–O type bonds) had lower net atomic charge than boron atoms surrounded by only three oxygen atoms (forming B \cdots O type bonds) as was expected.

One of the convenient tools for analyzing the experimental electron density is the localized-orbital locator (LOL). In a nutshell, it is a function introduced by Schmider and Becke which gives a measure of the relative velocity of electrons at a point r

$$\nu(r) = t(r)/[1 + t(r)]$$

where t stands for a dimensionless variable dependent on local kinetic energy densities.^{30,31}

$\nu(r)$ can obtain values within the range $0 \leq \nu \leq 1$. When the value is higher than 0.5, the space is associated with localized orbitals, whereas for values smaller than 0.5, the space is associated with the ionic and van der Waals bonds. The results of the LOL calculations presented in this paper are con-



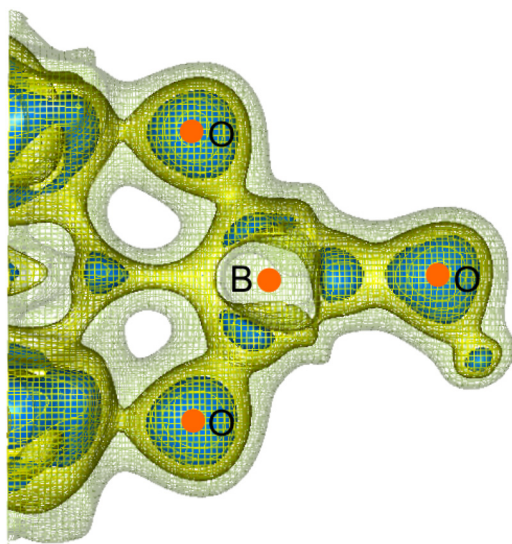


Fig. 6 Localized-orbital locator in the vicinity of the B(3) atomic position. Electron concentrations of $\nu = 0.483$ are depicted as the greenish mesh, electron concentrations of $\nu = 0.4915$ are depicted as the yellowish mesh and electron concentrations of $\nu = 0.496$ are shown as blue surfaces. Atomic positions are depicted as orange balls.

ducted according to the approach proposed by Tsirelson and Stash, where instead of the kinetic energy density calculated directly from Hartree–Fock wave functions, the kinetic energy density is obtained from the Hartree–Fock electron density.^{32–34} It is clearly seen in Fig. 6 that the values of ν between the B and O atoms are lower than 0.5, which is expected for the ionic bonds and consistent with the information about BCPs' topological properties (positive value of Laplacian).

Conclusions

To the best of our knowledge, the $\text{H}_4\text{B}_4\text{O}_9^{2-}$ ion is the first case when the experimental charge density distribution differences between B–O and B \cdots O have been shown and confirmed. Experimental results were consistent with complementary theoretical calculations and with literature data presenting theoretical results. From this investigation we have confirmed that topological indicators such as the values of the electron density and its Laplacian at the bond critical point can clearly determined whether the boron oxygen interaction is a B–O type or a B \cdots O type. For B–O electron densities, ρ had a value of *ca.* 1.0–1.25 (e \AA^{-3}) and the Laplacian $\nabla^2\rho$ was lower than 10 (e \AA^{-5}). For B \cdots O, the ρ value was *ca.* 1.4–1.5 (e \AA^{-3}) and $\nabla^2\rho$ was expected to be significantly higher than 10 (e \AA^{-5}).

Author contributions

Roman Gajda: investigation, data curation, visualization, writing – original draft, methodology, and formal analysis;

Anna Piekara: investigation and validation; Daniel Tchoń: formal analysis and visualization; Krzysztof Woźniak: validation, funding acquisition, and writing – review & editing; Wojciech A. Sławiński: conceptualization, resources, writing – review & editing, supervision, and funding acquisition.

Conflicts of interest

There are no conflicts to declare.

Acknowledgements

This work has been financially supported by the National Science Centre, Poland (project number 2018/31/B/ST4/00943). The authors also thank “Excellence Initiative – Research University (2020–2026)” at the University of Warsaw for the laboratory diffractometer upgrade (HyPix-6000HE detector). The authors also thank Anna Makal (Faculty of Chemistry, University of Warsaw) for fruitful discussions.

References

- 1 D. K. Straub, Lewis Structures of Boron Compounds Involving Multiple Bonding, *J. Chem. Educ.*, 1995, **72**, 494.
- 2 G. Mierzwa, A. J. Gordon, Z. Latajka and S. Berski, On the multiple BO bonding using the topological analysis of Electron Localisation Function (ELF), *Comput. Theor. Chem.*, 2015, **1053**, 130–141.
- 3 M. Michalski, A. J. Gordon and S. Berski, Theoretical insights and quantitative prediction of the nature of boron–chalcogen (O, S, Se, Te) interactions using the electron density and the electron localisation function (ELF), *Polyhedron*, 2021, **210**, 115495.
- 4 S. F. Matar and J. Etourneau, Electronic and Magnetic Structures of New Interstitial Boron Sub-Oxides B12O2:X (X = B, C, N, O), *Molecules*, 2021, **26**(1), 123.
- 5 M.-J. Valero-Pedraza, D. Alligier, E. Petit, D. Cot, D. Granier, K. Adil, P. G. Yot and U. B. Demirci, Diammonium tetraborate dihydrate as hydrolytic by-product of ammonia borane in aqueous alkaline conditions, *Int. J. Hydrogen Energy*, 2020, **45**, 9927–9935.
- 6 F. H. Stephens, V. Pons and R. Tom Baker, Ammonia–borane: the hydrogen source par excellence?, *Dalton Trans.*, 2007, 2613–2626.
- 7 Xcalibur/SuperNova CCD System, CrysAlisPro Software System.
- 8 G. M. Sheldrick, A short history of SHELX, *Acta Crystallogr., Sect. A: Found. Crystallogr.*, 2008, **64**, 112–122.
- 9 G. M. Sheldrick, Crystal structure refinement with SHELXL, *Acta Crystallogr., Sect. C: Struct. Chem.*, 2015, **71**, 3–8.
- 10 O. V. Dolomanov, L. J. Bourhis, R. J. Gildea, J. A. K. Howard and H. Puschmann, OLEX2: a complete structure solution, refinement and analysis program, *J. Appl. Crystallogr.*, 2009, **42**, 339–341.



- 11 N. K. Hansen and P. Coppens, Testing aspherical atom refinements on small-molecule data sets, *Acta Crystallogr., Sect. A: Cryst. Phys., Diffraction, Theor. Gen. Crystallogr.*, 1978, **34**, 909–921.
- 12 T. S. Koritsanzky and P. Coppens, Chemical Applications of X-ray Charge-Density Analysis, *Chem. Rev.*, 2001, **101**, 1583–1628.
- 13 A. Volkov, P. Macchi, L. J. Farrugia, C. Gatti, P. Mallinson, T. Richter and T. Koritsanzky, *XD2016 – A Computer Program Package for Multipole Refinement, Topological Analysis of Charge Densities and Evaluation of Intermolecular Energies from Experimental and Theoretical Structure Factors*, 2016.
- 14 A. Ø. Madsen, SHADE web server for estimation of hydrogen anisotropic displacement parameters, *J. Appl. Crystallogr.*, 2006, **39**, 757–758.
- 15 R. Dovesi, *et al.*, CRYSTAL17 User's Manual, *Wiley Interdisciplinary Reviews: Computational Molecular Science*, 2018.
- 16 R. Dovesi, A. Erba, R. Orlando, C. M. Zicovich-Wilson, B. Civalleri, L. Maschio, M. Rérat, S. Casassa, J. Baima, S. Salustro and B. Kirtman, Quantum-mechanical condensed matter simulations with CRYSTAL, *Wiley Interdiscip. Rev.: Comput. Mol. Sci.*, 2018, **8**, e1360.
- 17 A. D. Becke, Density-functional thermochemistry. III. The role of exact exchange, *J. Chem. Phys.*, 1993, **98**, 5648–5652.
- 18 C. Lee, W. Yang and R. G. Parr, Development of the Colle-Salvetti correlation-energy formula into a functional of the electron density, *Phys. Rev. B: Condens. Matter Mater. Phys.*, 1988, **37**, 785–789.
- 19 S. Grimme, J. Antony, S. Ehrlich and H. Krieg, A consistent and accurate ab initio parametrization of density functional dispersion correction (DFT-D) for the 94 elements H-Pu, *J. Chem. Phys.*, 2010, **132**, 154104.
- 20 D. Vilela Oliveira, J. Laun, M. F. Peintinger and T. Bredow, BSSE-correction scheme for consistent gaussian basis sets of double- and triple-zeta valence with polarization quality for solid-state calculations, *J. Comput. Chem.*, 2019, **40**, 2364–2376.
- 21 A. Erba, M. Ferrabone, R. Orlando and R. Dovesi, Accurate dynamical structure factors from ab initio lattice dynamics: The case of crystalline silicon, *J. Comput. Chem.*, 2013, **34**, 346–354.
- 22 C. Gatti and S. Casassa, *TOPOND14 User's Manual*, 1990.
- 23 C. Gatti, V. R. Saunders and C. Roetti, Crystal field effects on the topological properties of the electron density in molecular crystals: The case of urea, *J. Chem. Phys.*, 1994, **101**, 10686–10696.
- 24 R. F. W. Bader, *Atoms in Molecules: A Quantum Theory*, Oxford University Press, 1994.
- 25 R. F. W. Bader, A Bond Path: A Universal Indicator of Bonded Interactions, *J. Phys. Chem. A*, 1998, **102**, 7314–7323.
- 26 K. Durka, R. Kamiński, S. Luliński, J. Serwatowski and K. Woźniak, On the nature of the B..N interaction and the conformational flexibility of arylboronic azaesters, *Phys. Chem. Chem. Phys.*, 2010, **12**, 13126–13136.
- 27 K. N. Jarzemska, R. Kamiński, K. Durka and K. Woźniak, Ground-State Charge-Density Distribution in a Crystal of the Luminescent ortho-Phenylenediboronic Acid Complex with 8-Hydroxyquinoline, *J. Phys. Chem. A*, 2018, **122**, 4508–4520.
- 28 A. H. Reshak, X. Chen, S. Auluck and H. Kamarudin, Structural, electronic properties and charge density distribution of the LiNaB4O7: Theory and experiment, *Mater. Chem. Phys.*, 2012, **137**, 346–352.
- 29 V. R. Hathwar, A. K. Paul, S. Natarajan and T. N. Guru Row, Charge Density Analysis of a Pentaborate Ion in an Ammonium Borate: Toward the Understanding of Topological Features in Borate Minerals, *J. Phys. Chem. A*, 2011, **115**, 12818–12825.
- 30 H. Schmider and A. Becke, Chemical content of the kinetic energy density, *J. Mol. Struct.: THEOCHEM*, 2000, **527**, 51–61.
- 31 H. L. Schmider and A. D. Becke, Two functions of the density matrix and their relation to the chemical bond, *J. Chem. Phys.*, 2002, **116**, 3184–3193.
- 32 V. Tsirelson and A. Stash, Determination of the electron localization function from electron density, *Chem. Phys. Lett.*, 2002, **351**, 142–148.
- 33 A. Stash and V. Tsirelson, Modern possibilities for calculating some properties of molecules and crystals from the experimental electron density, *Crystallogr. Rep.*, 2005, **50**, 177–184.
- 34 A. I. Stash and V. G. Tsirelson, Developing WinXPRO: a software for determination of the multipole-model-based properties of crystals, *J. Appl. Crystallogr.*, 2014, **47**, 2086–2089.
- 35 R. W. W. Hooft, L. H. Straver and A. L. Spek, *J. Appl. Crystallogr.*, 2010, **43**, 665–668.

